The Application of Radio Diagnostics to the Study of the Solar Drivers of Space Weather

Alexander Warmuth and Gottfried Mann

Astrophysikalisches Institut Potsdam, An der Sternwarte 16, D-14482 Potsdam, Germany

Summary. The application of radio observations to the study of the solar drivers of space weather – flares and CMEs – is reviewed. The different radio emission mechanisms relevant in the solar corona and in interplanetary space are discussed, with an emphasis on plasma emission. The principal types of instrumentation used are presented, as well as some basic techniques which can be applied to extract information from the obtained data. The different kinds of solar radio bursts (intense non-thermal radio emission features observed in dynamic radio spectra) are discussed. They are categorized according to the observing frequency range and with respect to their spectral characteristics. Finally, the different applications of radio data to space weather studies are reviewed: radio observations can be used to study the underlying physics of solar eruptive events, they can be correlated with effects at the Earth in order to forecast space weather hazards, and they allow the study and tracking of potentially geo-effective disturbances (interplanetary coronal mass ejections and shock waves) from the Sun through interplanetary space to the Earth.

1 Introduction

Solar eruptive events – mainly *flares* and *coronal mass ejections (CMEs)* – are the main drivers of space weather. A general scheme of how these phenomena can potentially influence the geomagnetic environment of the Earth is shown in Fig. 1 (here we restrict ourselves to particles and bulk mass motions, omitting the various effects due to flare-generated energetic electromagnetic radiation). The geo-effective agents are generated at the Sun, they propagate through the interplanetary (IP) medium, and finally interact with the Earth's magnetosphere.

Shock waves which propagate away from the Sun are launched by flares and/or fast CMEs. A fraction of the shocks (often the ones driven by CMEs) can penetrate into the IP medium (where they are called *IP shocks*) and reach the Earth. At these shocks, particles can be accelerated to high energies, creating *gradual solar energetic particle (SEP) events* which may have severe geo-effective consequences. Alternatively, particles can be directly accelerated

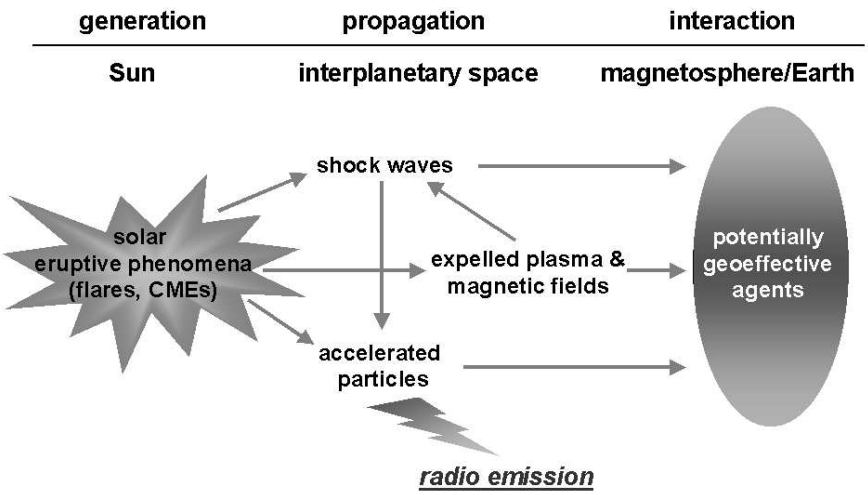

Fig. 1. General scheme of the interactions relevant for space weather: solar eruptive events are produced at the Sun (*left*), the disturbances they create propagate through the interplanetary medium (*middle*) and finally interact with the Earth's magnetosphere (*right*).

in the impulsive phase of a flare, and provided they encounter open magnetic field lines, they can escape and propagate into the IP medium. These *impulsive SEP events* are more frequent than the gradual ones, but are less important in terms of space weather. For a comprehensive review of both types of SEP events, see Reames (1999).

The matter and magnetic fields that are expelled from the corona by CMEs propagate through the IP medium, where they are called ICMEs or, if measured in-situ, magnetic clouds (Burlaga et al., 1981). They may interact with the Earth's magnetosphere, potentially producing a geomagnetic storm (which is most likely when the IP magnetic field has a southward component; see e.g. Chen et al. 1997), the most severe disturbance of the geomagnetic environment (e.g. Gosling 1993, Webb 1995).

As will be seen in Sect. 2, intense solar radio radiation – so-called *solar radio bursts* – can only be generated via a nonthermal mechanism which requires the presence of accelerated electrons. These electrons are either accelerated directly by flares, or by shock waves created by flares or CMEs. Therefore, radio observations provide a particularly valuable tool for studying the solar

drivers of space weather and the disturbances they are creating – coronal and IP shocks, energetic particles, and transient disturbances of the IP medium.

It should be noted that space weather is also significantly influenced by a process that is not connected to cataclysmic events at the Sun, but which is instead tied to the large-scale topology of its magnetic field. When fast solar wind streams, which originate from regions where the coronal magnetic field lines are open (coronal holes), overtake the slow solar wind component, co-rotating interaction regions (CIRs) are formed. Ahead and behind a CIR, a pair of shocks is formed in this process, at which particles can be accelerated (see, e.g., Mann et al. 2002 and references therein). This mechanism is responsible for quasi-periodic geomagnetic disturbances, while flares and CMEs cause sporadic – and at times severe – geomagnetic effects. We will concentrate on the latter case.

2 The Physics of Solar Radio Emission

2.1 Emission Mechanisms

The Sun is the brightest radio source in the sky. Three different emission mechanisms contribute to the solar radio flux, and which one is dominating depends on the observing frequency and the solar activity. The first component is *thermal free-free emission*, also known as *thermal bremsstrahlung*. It is generated by free electrons (with a Maxwellian distribution function) which are deflected by the Coulomb electric fields of ions. Thermal emission is dominant in the quiet Sun.

The second important emission mechanism on the Sun is *gyro emission*, which operates through the spiraling motion of the electrons along magnetic field lines at the electron gyrofrequency,

$$\omega_{\mathrm{ge}} = \frac{eB}{m_{\mathrm{e}}} \,, \tag{1}$$

where e is the elementary charge, m_{e} the electron mass, and B the magnetic field strength in Teslas. Depending on whether the electrons are non-relativistic, mildly relativistic, or highly relativistic, this mechanism is called *cyclotron*, *gyrosynchrotron*, or *synchrotron emission*, respectively. Of these, only cyclotron and gyrosynchrotron emission are important in the context of solar activity: the former is responsible for the bright coronal emission above sunspots (where B is strong), while the latter dominates the high-frequency bursts associated with solar flares (see Sect. 4.1). Gyrosynchrotron emission is emitted at ω_{ge} and its harmonics, with the contribution of a continuum due to line broadening.

Both thermal bremsstrahlung and gyro emission are *incoherent* processes, which means that the electrons act independently to produce radiation. The observed brightness temperature is then dependent on the kinetic temperature

of the particles. However, electrons can also be accelerated in phase, producing photons which are also in phase. This *coherent emission* can have much higher brightness temperatures (up to 10^{15} K). On the Sun, coherent radiation is mainly due to *plasma emission*.

2.2 Plasma Emission

On the Sun, plasma emission is predominantly occurring at frequencies below 1 GHz. The dominance of plasma emission in active events is dramatically shown by the following comparison: while the thermal emission of the quiet Sun amounts to a flux of 3 sfu (*solar flux units*, 1 sfu = 10^{-22} W m^{-2} Hz^{-1}) at 40 MHz, a typical radio burst produces a flux of 10^5 sfu at the same frequency.

Let us consider a simple 1D model of an electron embedded in a plasma. In perfect equilibrium, the electric fields of the positive and negative charges will cancel out, but when the electron is displaced from its equilibrium position, it will feel a net electric field E along the x-direction. The force F acting on the electron is given by the equation of motion,

$$F = m_\mathrm{e}\ddot{x} = -eE \,, \tag{2}$$

where m_e is the electron mass and x the displacement from the equilibrium position. The field E is generated by the background distribution of the other charged particles in the plasma, which is represented by the charge density, ϱ. The relation between the two variables is given by Poisson's equation,

$$div\ \boldsymbol{D} = \varrho \,, \tag{3}$$

where $\boldsymbol{D}$ is the displacement vector. In our model, this simplifies into

$$\frac{\mathrm{d}E}{\mathrm{d}x} = \frac{eN_e}{\varepsilon_0} \,, \tag{4}$$

where N_e is the total electron number density and ε_0 the permittivity of vacuum. Here, the ions are considered to be immobile due to their high mass with respect to the electron mass. Substituting (4) into (2) then gives

$$\ddot{x} + \frac{e^2 N_e}{\varepsilon_0 m_\mathrm{e}} x = 0 \,. \tag{5}$$

Equation 5 describes a classical oscillator. The electron undergoes a harmonic oscillation with the circular frequency

$$\omega_\mathrm{pe} = \sqrt{\frac{e^2 N_e}{\varepsilon_0 m_\mathrm{e}}} \,, \tag{6}$$

which is called the *electron plasma frequency* (often, $f_{pe} = \omega_{pe}/2\pi$ is used instead). This is the natural frequency of electrostatic oscillations of electrons in a plasma.

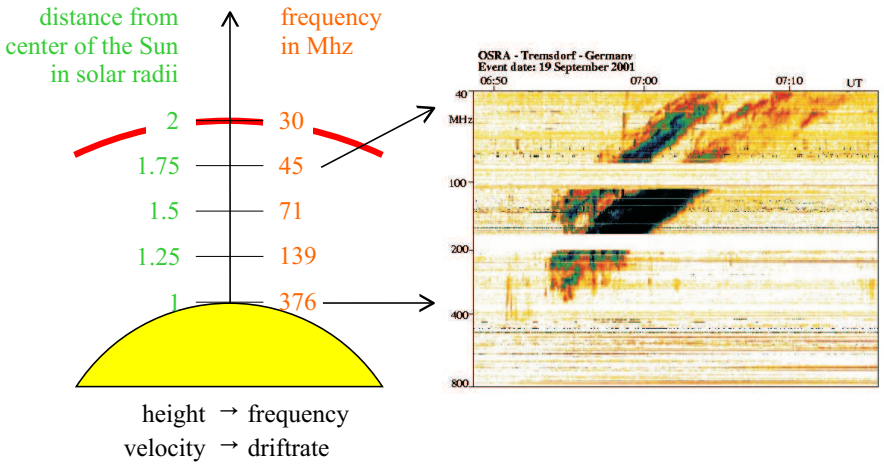

Fig. 2. Schematic of the solar corona (*left*) showing a scale indicating the distance from the center of the Sun (in solar radii; 1 $R_s = 6.96{\cdot}10^5$ km), and the corresponding plasma frequencies (in MHz) as given by the twofold Newkirk density model (see main text). Using this frequency-height relation, a dynamic radiospectrum (*right*) can be converted to a height-time plot.

Plasma emission works in the following way. The plasma is externally disturbed (e.g. by an electron beam or a shock wave) so that the electrons are excited to oscillate. Then, these electrons emit radio waves. In contrast to gyrosynchrotron emission, where the electrons individually generate radio waves, the electrons of the whole plasma *collectively* emit radio waves in the case of plasma emission.

In a plasma, a large variety of wave modes is present. For our purposes, we are especially interested in *Langmuir waves*, which are high-frequency electron plasma oscillations modified by the thermal motions of the electrons. Langmuir waves have a frequency slightly above f_{pe} and can be excited by suprathermal electrons. Subsequently, Langmuir waves can be converted into escaping electromagnetic waves by scattering at ion density fluctuations and/or by coalescence with low frequency plasma waves (ion acoustic waves). This mechanism generates the fundamental emission near the plasma frequency f_{pe}, while harmonic emission (usually near $f = 2f_{pe}$) arises from the coalescence of two high-frequency electrostatic waves (e.g. Melrose 1985). This rather complicated, non-linear process is referred to as plasma emission.

2.3 Derivation of Radio Source Heights and Speeds

The frequency at which plasma emission occurs is directly proportional to the square root of the electron number density, N_e. A convenient form of (6) is

$$f_{\rm pe} = \omega_{\rm pe}/2\pi \approx 9 \times N_e^{1/2} \,, \tag{7}$$

with N_e given in units of m^{-3}. The coronal (and IP) electron density, on the other hand, is a function of height above the solar surface, with N_e monotonically decreasing with height. Each layer in the solar atmosphere therefore corresponds to a characteristic f_{pe}. When we observe a plasma emission feature and apply a suitable coronal electron density model, we can then derive the height of the emission source above the solar surface. For example, frequencies of hundreds of MHz correspond to the low corona, while emission at 20 kHz occurs at one astronomical unit (see Sect. 4.1).

A motion of the source towards, say, greater heights, will then be observed as a drift of the emission towards lower frequencies, since N_e drops with increasing height. The relationship between the drift rate D_f at the frequency f and the radial source velocity v_{source} is given by

$$D_f = \frac{\mathrm{d}f}{\mathrm{d}t} = \frac{f}{2}\frac{1}{N_e}\frac{\mathrm{d}N_e}{\mathrm{d}t}v_{\mathrm{source}} \tag{8}$$

A commonly used coronal density model was derived by Newkirk (1961):

$$N_e(R) = \alpha\, N_0\, 10^{4.32 R_{\mathrm{S}}/R}\ . \tag{9}$$

It gives the electron number density N_e as a function of radial distance R from the solar surface (normalized to the solar radius R_S), with $N_0 = 4.2{\cdot}10^{10}\,\mathrm{m}^{-3}$, and the enhancement factor $\alpha = 1 - 4$ (dependent on whether the burst takes place in the quiet corona or near an active region). The Newkirk model corresponds to a barometric height behavior of the gravitationally stratified corona with a temperature of 1.4 MK (see Koutchmy 1994). A heliospheric density model, which is especially useful when dealing with IP phenomena, has been developed by Mann et al. (1999).

Summarizing, each frequency corresponds to a height in the solar atmosphere, and each drift rate to a source velocity. The diagnostic tool which is employed to derive these parameters is the *dynamic radio spectrum*. It represents the intensity of the received radiation in terms of time t and frequency f. In such a spectrum, t runs from left to right, while f decreases from bottom to top, corresponding to increasing height (for a graphic representation, see Fig. 2). Thus, the dynamic radio spectrum represents a path-time diagram of the radio source.

3 Instrumentation and Observational Techniques

The incoming solar radio flux can be characterized by $I = I(f, \theta, \phi, t)$, that is, the intensity I (also known as *flux density*) as a function of frequency f, angular directions θ and ϕ in the plane of the sky, and time t. In addition, the radiation may be polarized, which means that in principle all four Stokes parameters could be defined by f, θ, ϕ, and t. Solar radio telescopes can measure a subset of these parameters of the incoming radiation. For the sake

of brevity, let us just consider the total intensity I, bearing in mind that many instruments are capable of measuring additional Stokes parameters (usually V, the degree of circular polarization).

The most basic instrument is the *radiometer*, which just measures the flux density $I = I(t)$, at a fixed frequency and averaged over the whole Sun. The principal advantages of radiometers are their simplicity and high time cadences.

A *radiospectrograph* is capable of obtaining dynamic radiospectra $I = I(f, t)$ and could be regarded as a combination of many radiometers at different, closely spaced frequencies. Today, radiospectrographs observing from the microwave range up to the kilometer regime represent the main asset of solar radio astronomy. A typical example is the Potsdam-Tremsdorf radiospectropolarimeter (Mann et al. 1992), which measures the solar radio flux in 1024 channels from 800 down to 40 MHz, with a temporal resolution of 0.1 s.

Radioheliographs obtain 2-D radio images of the Sun at one or several fixed frequencies, $I = I(\theta, \phi, t)$, utilizing interferometric techniques. Radioheliograms thus complement the spectral data. Two such instruments which have significantly advanced our knowledge of the radio Sun are the Nançay radioheliograph (Kerdraon and Delouis 1997), which observes at five different frequencies in the metric range (164, 237, 327, 411, and 432 MHz), and the Nobeyama radioheliograph (Nakajima et al. 1994), which operates at two centimeter wavelengths (17 and 34 GHz). Both instruments image the full Sun, the angular resolutions range from 10" at cm wavelengths up to 10' for the metric range.

Finally, it should be noted that ground-based radio observations are only possible above the ionospheric cut-off frequency ($\nu \simeq 7$ MHz), and are already extremely difficult below 20 MHz due to terrestrial interference. Since plasma emission at and below these frequencies originates from IP space, radio instruments have to be space-borne in order to study this regime which is of special importance with respect to space weather. A multitude of spacecraft have been carrying radio receivers, the most important instrument currently being the WAVES radiospectrograph aboard the *Wind* spacecraft (Bougeret et al. 1995). WAVES covers the dekametric/hectometric/kilometric range from 14 MHz down to 4 kHz.

4 Solar Radio Bursts

We will now discuss the solar radio signatures which are connected with solar eruptive events and which are thus of particular relevance in the context of space weather. Our focus is therefore on the nonthermal solar radio bursts, which are usually generated by plasma emission. Radio bursts are normally classified according to two criteria: the wavelength of observation and the morphological appearance in dynamic radio spectra. These different classification

schemes are discussed below, with an emphasis on the underlying physical processes.

4.1 Wavelength Regimes

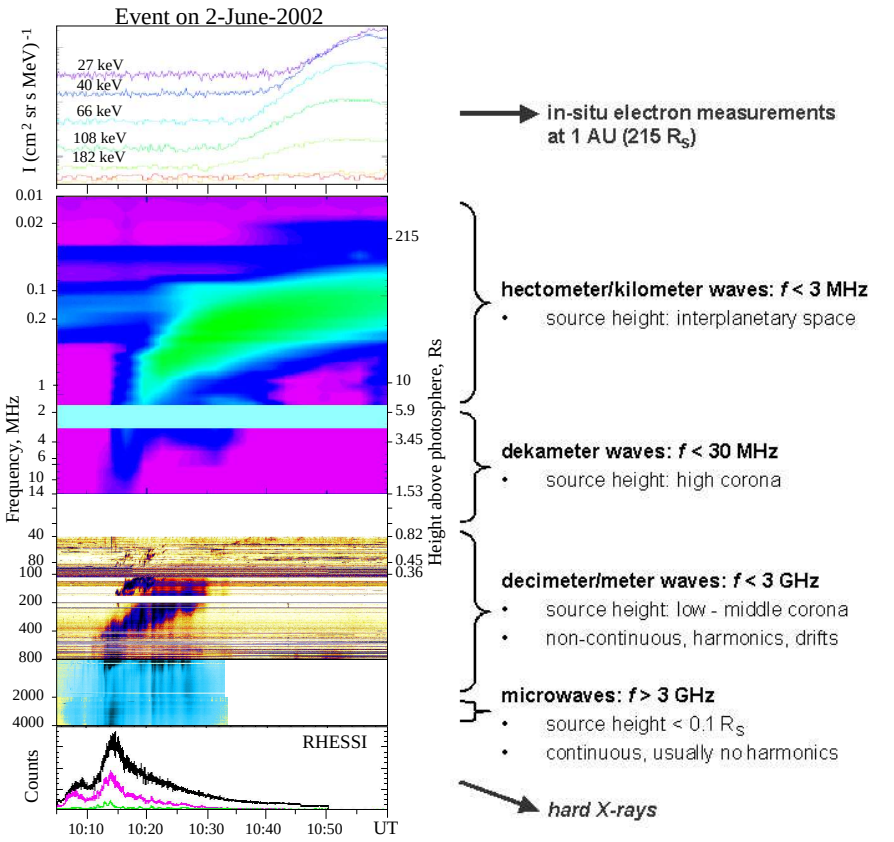

Fig. 3. The solar eruptive event of 2 June 2002 (adapted from Classen et al. 2003). *Bottom*: hard X-ray count rates (RHESSI). *Middle*: combined dynamic radiospectrum (see main text for details). Frequency decreases from bottom to top (corresponding to increasing height in the solar atmosphere). *Top*: In-situ electron flux measurements (*Wind*/3DP) at different energies. The text to the right of the graph gives some basic information on the radio wavelength ranges.

In order to illustrate the different wavelength ranges, as well as the corresponding source heights, Fig. 3 shows a combined solar radio spectrum from the solar eruptive event of 2 June 2002 (see Classen et al. 2003). The three spectra were provided by the Ondřejov radiospectrograph (4 GHz to 800 MHz,

see Jiricka et al. 1993), the Potsdam-Tremsdorf radiospectropolarimeter (800 MHz to 40 MHz, see Mann et al. 1992), and by *Wind*/WAVES (14 MHz to 10 kHz, see Bougeret et al. 1995). In addition, the lowermost and the uppermost parts of Fig. 3 show hard X-ray (HXR) fluxes obtained with the Reuven Ramaty High Energy Solar Spectroscopic Imager (RHESSI; see Lin et al. 2002) and in-situ measurements of electron fluxes provided by the 3-D Plasma and Energetic Particles Detector (3DP; see Lin et al. 1995) aboard the *Wind* spacecraft, respectively.

As is the convention for solar radiospectrograms, time runs from left to right and frequency decreases from bottom to top (corresponding to increasing height). In the following, we examine the different spectral regimes, starting at the highest frequencies (i.e. the lowest heights).

Microwaves ($f > 3$ GHz)

They originate low in the corona and/or in the chromosphere (at heights of $h < 0.1\ R_S$). Microwave emission is generally broad-band and continuous (i.e. there are no fine structures). Most of the microwave bursts are due gyrosynchrotron emission by relativistic electrons. Microwave bursts are often closely correlated with the flare's HXR emission (see the HXR lightcurves in Fig. 3), which implies that they are generated by the same energetic electron population that produces the HXR bremsstrahlung – the same particle population that contains the bulk of the energy released in the flare. Therefore, microwave observations of flares provide important information on the primary particle acceleration mechanisms.

Decimeter/meter waves ($f < 3$ GHz)

This remains the best-studied wavelength regime. Radiation in this range is coming from the low and the middle corona ($h \simeq 1\ R_S$), respectively. In contrast to microwaves, most of the emission is non-continuous, it can be narrow-band, and a multitude of distinct fine structures, harmonics and frequency drifts is observed. The high fluxes and brightness temperatures of the observed bursts require a coherent emission mechanism – namely plasma emission.

Dekameter waves ($f < 30$ MHz)

The dekametric regime is generally similar to the metric, but it originates from the higher corona. Emission mechanisms and morphologies of bursts are also similar. Observations in the dekametric band provide an important link between the comparatively well-known middle corona and the IP space.

Hectometer/kilometer waves ($f < 3$ MHz)

With respect to emission mechanisms and morphology of bursts, this range is also similar to the meter/dekameter bands. However, as these extremely

long wavelengths correspond to the plasma frequency of the IP medium, they are of particular interest in the context of space weather. Observations in this regime allow the tracking of disturbances from the high corona up to the Earth (and even beyond it), which will not be possible with any other kind of observational technique until the Solar Mass Ejection Imager (SMEI; see Radick 2001) becomes fully operational.

4.2 Types of Solar Radio Burst

We now proceed to the classification of solar radio bursts according to their appearance in dynamic radiospectra. Note that although this classification was devised for meter-wave bursts, it can be applied to a significantly wider wavelength range (decimetric to kilometric). Figure 4 is an idealized dynamic radio spectrum and shows the basic types of solar radio bursts (as in Fig. 3, frequency decreases from bottom to top). Important characteristics of the bursts are their duration Δt, their bandwidth Δf, and their drift rate, $D_f = \mathrm{d}f/\mathrm{d}t$. In the following, the numerical values given for these parameters will be referring to the metric range. An excellent discussion of the meter-wave bursts can be found in Mclean and Labrum (1985).

It is generally accepted that all following bursts are generated by plasma emission (though at least some type IV bursts may be due to gyrosyncrotron emission). The microwave bursts (μ in Fig. 4), which are due to other mechanisms, have already been discussed in Sect. 4.1.

Type I Bursts

Type I bursts (Fig. 5) are characterized by a very short duration (< 1 s), they have bandwidths of a few tens of MHz, and they do not show obvious drifts. Type I bursts are only observed at metric wavelengths and always appear in large numbers, forming irregular structures superposed on a continuous background. These so-called *noise storms* can last for hours to days. Type I emission is therefore not necessarily associated with flares. It is thought to be generated by electrons accelerated to a few thermal energies by an ongoing local energy release in closed coronal structures. Type I bursts are not particularly important for space weather studies, therefore, we will refrain from an in-depth discussion.

Type II Bursts

Type II bursts (Fig. 5) are narrow-band (a few MHz) emission lanes which slowly drift towards lower frequencies ($D_f \simeq 0.1 - 1$ MHz s^{-1}). Both fundamental and harmonic band can be present, and sometimes each band is split into a higher and a lower frequency lane (with a relative separation of $\Delta f/f \simeq 0.1$). For a review, see Mann (1995). Most bursts are observed in the metric range, but some are also detected in the dekametric to kilometric regimes. These are called IP type II bursts (see, e.g., Cane et al. 1987).

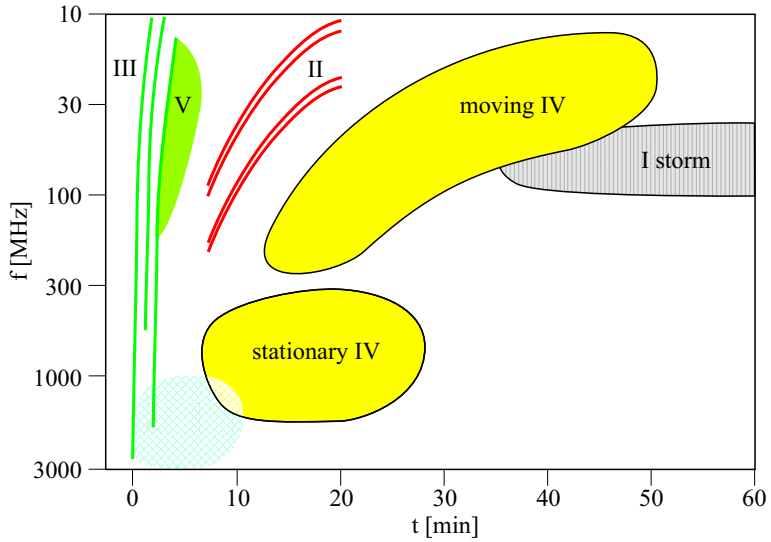

Fig. 4. Dynamic solar radio spectrum showing schematically the basic types of solar radio bursts. Time runs from left to right, frequency decreases from bottom to top (corresponding to increasing height in the solar atmosphere). Time is given in minutes, frequency in MHz.

A type II burst is generated by a magnetohydrodynamic shock wave which propagates outward through the corona. In the corona and in the IP medium, a type II-generating shock is formed when a disturbance exceeds the Alfvén speed

$$v_{\mathrm{A}} = \frac{B}{\sqrt{\mu_0 m_{\mathrm{p}} \mu N}} \,, \tag{10}$$

where μ_0 is the permeability of vacuum, m_p the proton mass, μ the mean molecular weight (0.6 in the corona), and N the total particle number density ($N = 1.92\, N_e$ for $\mu = 0.6$). Velocities of coronal type II sources are of the order of 1000 $\mathrm{km\,s^{-1}}$. At the shock front, electrons are accelerated to suprathermal and/or high energies. They excite Langmuir waves which are then converted into escaping radio waves by the plasma emission process outlined in Sect. 2.2.

Further evidence for electron acceleration is provided by the *herringbone structure* observed in some type II bursts, in which small type III-like bursts (see below) emanate from the "backbone" of the emission lane. These features are interpreted as accelerated electrons which escape from the shock.

Type II bursts are associated both with flares and CMEs, though there is no one-to one correspondence. This has resulted in an extended discussion on the real nature of the shocks which produce the bursts, the candidates being a flare-generated pressure pulse (see e.g. Vršnak and Lulić 2000a; Vršnak and Lulić 2000b) or a piston-driven shock created by a CME (Cliver et al. 1999 and

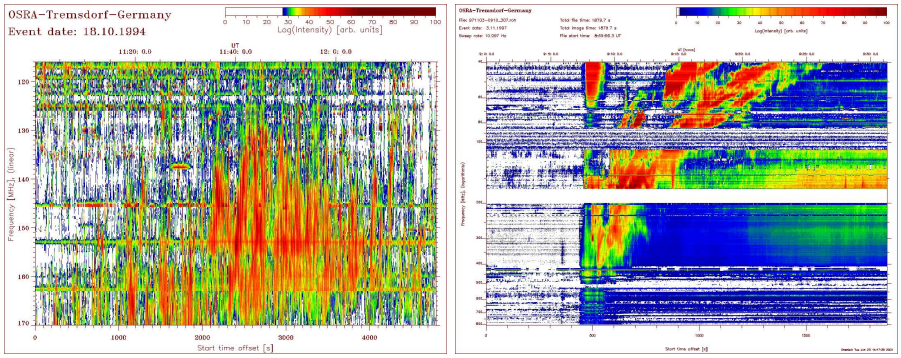

Fig. 5. Dynamic spectra of solar radio bursts (Potsdam-Tremsdorf radiospectropolarimeter). *Left*: A group of type I bursts. Together, they form a noise storm. The individulal bursts are irregularly distributed in frequency and time, no systematic drifts are evident, and the duration of each busrst is very short. *Right*: Type II burst. Note the gradual drift from higher to lower frequencies, the fundamental-harmonic stucture of the two emission lanes, and the band-splitting evident in both of the lanes. The white horizontal bar is a data gap.

references therein). The current view is that both flares *and* CMEs can create shocks (e.g. Classen and Aurass 2002; Shanmugaraju et al. 2003), but it seems that the flare-generated disturbances usually cannot penetrate to IP space, since most of those bursts cease at $\simeq$ 20 MHz (Gopalswamy et al. 1998b). This is probably due to a local maximum of the Alfvén speed in the higher corona (Mann et al. 2003). Therefore, most hectometric/kilometric type II bursts seem to be generated by CME-driven shocks (Cane et al. 1987). These bursts are associated with fast CMEs, long-lived energetic solar particle events (Kahler et al. 2003), and IP shocks, and are therefore particularly relevant for space weather purposes.

Type III Bursts

Type III bursts (Fig. 6) are the most common flare-associated bursts and can occur over a wide frequency range, from $\simeq$ 1 GHz to $\simeq$ 10 kHz, corresponding to a height range extending from the low corona to beyond 1 AU. They are mainly defined by their rapid drift ($D_f \simeq 100\,\mathrm{MHz\,s^{-1}}$) towards lower frequencies, they have a short duration (seconds) and a relatively broad bandwidth ($\Delta f \simeq 100\ \mathrm{MHz\,s^{-1}}$). Many type III bursts display harmonic structure at metric to dekametric wavelengths.

Type III bursts are characteristic of the impulsive phase of solar flares, where they often occur in groups of $\simeq$ 10 bursts, lasting a few minutes. Non-flare associated type IIIs form storm type III bursts, somewhat reminiscent of type I noise storms. The exciting agent of a type III burst is a beam of mildy relativistic electrons ($v \simeq 0.3\,c$) which propagates out of the corona along open magnetic field lines (the beams may also propagate in closed loops, resulting

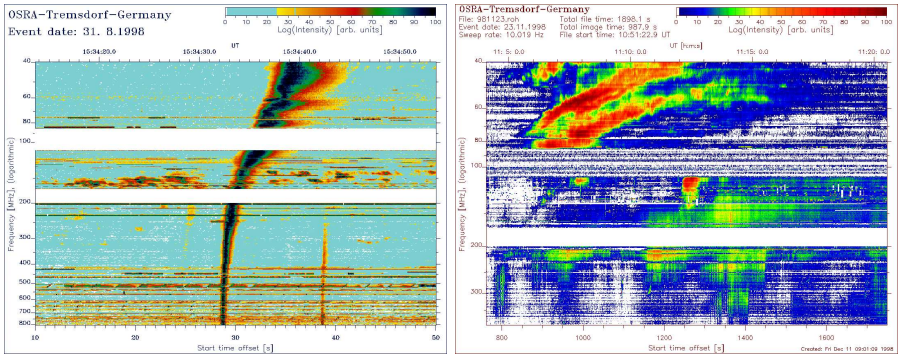

Fig. 6. Dynamic spectra of solar radio bursts (Potsdam-Tremsdorf radiospectropolarimeter). *Left*: Type III burst. It displays a rapid frequency drift and has a short duration. *Right*: Type IV burst (in the lower part of the spectrum). Note the broadband structure and the slow drift towards lower frequencies. The feature in the upper left of the spectrum is a well-defined type II burst.

in so-called *inverted-U bursts*). As in the case of type II bursts, the accelerated electrons generate plasma emission. Type III bursts can propagate through IP space up to the Earth, where the radio-generating electrons can be directly observed as *impulsive electron events*. Type III bursts therefore give vital clues on the acceleration of electrons in flares, as well as on the propagation of these particles through IP space.

A special class of type III bursts are the so-called *shock-accelerated (SA) type III bursts* (see Cane et al. 1981; Bougeret et al. 1998; Klassen et al. 2002). They start from a type II backbone and are somewhat reminiscent of herringbones, but contrary to them, SA type III bursts extend into the IP medium. Like the herringbones, they are thought to be generated by electron beams which are accelerated at a coronal (or IP) shock.

Type IV Bursts

Type IV bursts are flare-related broad-band continua (Fig. 6). They are divided into two distinct categories: *stationary type IV bursts* show no frequency drift and are characterized as broad-band, long-lasting continuum features which show a wide variety of fine structures – pulsations, zebra patterns and fiber bursts. They follow major flares and may evolve into type I storms. On the other hand, *moving type IV bursts* display a slow drift towards lower frequencies (corresponding to source velocities of up to several 100 $\mathrm{km\,s^{-1}}$), while they are otherwise morphologically similar to stationary type IVs.

Type IV bursts are believed to be either due to plasma emission or due to gyrosynchrotron emission. In any case, the electrons which are responsible for the emission are trapped in a closed magnetic structure. This can be a set of coronal loops (stationary type IV), or a rising structure like an expanding loop or a plasmoid which is ejected during an eruptive event (moving type IV; see,

e.g., Stewart 1985). The bulk of the electrons remains confined to the magnetic structure due to magnetic mirroring at converging magnetic field lines (i.e., at the feet of coronal loops), therefore, we observe prolonged emission.

Type IV bursts are only seldomly observed in the near-Sun IP medium, but they are nevertheless interesting for solar-terrestrial studies since they can provide valuable information on the energy release mechanism of solar eruptive events. Several flare models require the formation and ejection of plasmoids, and CME cores might actually be sources of type IV bursts.

Type V Bursts

Type V bursts are continuum bursts which start during or immediately after a group of type III bursts. They are possibly created by electrons which have been removed from the type III-generating beam by pitch angle scattering. For the purposes of solar-terrestrial studies, type V bursts are not important.

4.3 An Example – The Solar Eruptive Event of 2 June 2002

We return to Fig. 3 in order to show how observations in different wavelength ranges can be combined to track different radio sources from the lower corona to 1 AU. The event of 2 June 2002 was associated with a moderate C8/SF flare at the solar coordinates S20W61. This location near the west limb means that the event was magnetically well connected to the Earth.

The lowermost panel in Fig. 3 shows the count rate of HXR photons as measured by the RHESSI instrument (Lin et al. 2002) in the energy bands of 6-12, 12-25, and 25-50 keV (the higher the energy, the lower is the count rate). Radiation at these energies is primarily due to bremsstrahlung emitted by electrons which precipitate onto the chromosphere.

In the dynamic radio spectrum from 4 GHz to 800 MHz, several fast-drifting microwave bursts are visible. A closer examination shows that the bursts are temporally associated with the peaks of the HXR flux, which means that the radio-generating electrons are accelerated at the same site and by the same mechanism as the bremsstrahlung-emitting electron population is (see Classen et al. 2003).

In the range from 800 to 40 MHz, several radio bursts can be discerned: the big dark feature drifting from high to low frequencies is a moving type IV burst, while the smaller drifting feature at $\sim$ 150 MHz is the harmonic band of a type II burst. Just above it, the fundamental band is faintly visible (at $\sim$ 80 MHz). At $\sim$10:14 UT, a series of weak type III bursts is observed (beginning at $\sim$ 50 MHz). At lower frequencies (below 14 MHz), the type III bursts, having merged into a single burst, have become the dominating feature in the radiospectrum. From these observations, combined with Nançay radioheliograms, it was concluded that the type II-generating shock moved ahead of the type II source (presumably a plasmoid) at roughly the same velocity ($\sim 500\ \mathrm{km\,s^{-1}}$).

From the in-situ electron flux measurements (top panel in Fig. 3), it was found that the particles were injected at the Sun after *both* the primary energy release and the the shock wave development. However, there is a good temporal association with minor HXR peaks. It is concluded in Classen et al. (2003) that the high-energy electrons measured at the Earth are accelerated by an ongoing reconnection process in the low corona.

5 Applications of Radio Observations

After having discussed how radio emission is generated and which different kinds of signatures the active Sun creates, we will now show how this knowledge can be employed for the benefit of space weather studies. Basically, three different approaches are possible: radio observations can be used to study the underlying physics of solar eruptive events, they can be correlated with effects at the Earth in order to forecast space weather hazards, and they allow the study and tracking of potentially geo-effective disturbances from the Sun through the IP medium to the Earth.

5.1 Studying the Nature of Flares and CMEs

Radio observations can be used to study the basic nature of flares and CMEs, which includes the primary energy release and particle acceleration. Though this is not directly connected with space weather, it is nevertheless crucial, for without an understanding of the basic drivers of space weather, the reliability of any forecasts remains doubtful.

Since this approach is mainly concerned with the origin and initial development of flares and CMEs, its objects of study are close to the Sun, and consequently observations at the shorter wavelengths are required. Microwave observations can provide many important inferences on energy release and particle acceleration in flares, especially when combined with HXR data). For example, gyrosynchrotron emission from flares can be used to derive coronal magnetic field strengths (see, e.g., Gary and Hurford 1994).

With regard to the metric regime, several possibilities of analyzing radio bursts have already been mentioned in Sect. 4.2. Type III bursts offer us very sensitive diagnostics of coronal energy release and particle acceleration. Type II and type IV bursts can be used to study the propagation of coronal shocks (e.g. Vršnak et al. 2002a) and closed magnetic structures (i.e. CME cores or plasmoids, e.g. Gopalswamy et al. 1990), respectively, and can be used to derive important physical parameters of the corona. For example, if we accept that the band split observed in some type II bursts is due to emission from ahead of and behind the shock front (e.g. Smerd et al. 1975), then the amount of band split yields the compression factor $X = \varrho_d/\varrho_u$ (where ϱ_u is the upstream and ϱ_d the downstream density) at the shock. Using a simple model (Vršnak et al. 2002b), we can then deduce the Alfvénic Mach number

M_A of the shock and, taking the type II speed derived with a coronal density model, we get the Alfvén speed v_A and the magnetic field strength B of the ambient medium. The knowledge of these coronal parameters is vital for the understanding of how a CME develops, and how a coronal shock may penetrate into the IP medium.

Complementary to these spectral techniques, radioheliographic observations offer important inferences on the spatial and kinematic evolution of space weather agents. CMEs can be detected due to the non-thermal particles accelerated during the magnetic energy release. This is possible out to a few solar radii. In radioheliograms, CMEs can be observed also in front of the solar disk, which is not possible with coronagraphs. In addition, a much higher time cadence is possible with radioheliographs. Therefore, a more complete picture of the geometry of the CME and its trajectory is obtained (Kundu et al. 1989; Maia et al. 2000; Bastian et al. 2001; Manoharan et al. 2001), which is in turn vital for predicting the impact of the CME on the IP medium and, ultimately, on the Earth. The same technique can be applied to study the trajectories of type II, type III and type IV burst sources. One major result of these studies was that most type II bursts have clearly non-radial (with respect to the normal on the solar surface) trajectories (e.g. Stewart 1984; Aurass et al. 1998).

On the other hand, radioheliographs operating in the microwave range can observe CME-associated prominence eruptions and arcade formation (see Hanaoka et al. 1994; Gopalswamy et al. 1998a). All these phenomena are important to understand the mechanisms which lead to the launch of a CME. Note also that there are several additional phenomena that are associated with flares and/or CMEs, such as smaller-scale ejecta (e.g. flare sprays, see Vršnak 2001) or Moreton waves (e.g. Warmuth et al. 2001). On the one hand, such phenomena can be sources of shocks and may accelerate particles, while on the other hand they can offer diagnostic tools for studying the underlying physics of solar eruptions.

5.2 Using Radio Events as Predictors of Space Weather Hazards

Apart from being used to study the basic physics of solar eruptions, radio observations can directly be employed as a tool of space weather prediction. The principle here is to look for correlations between radio phenomena and effects at the Earth. The fast CMEs that drive IP shocks and produce SEP events are generally associated with metric/dekametric type II and type IV bursts, and we can use this correlation to predict the arrival of such geo-effective disturbances. While the correlation is quite coarse, which certainly does not allow straightforward prediction of potential geo-effectiveness, it is nevertheless an additional channel of information for space weather forecasting, and combined with other data sets (particularly optical, extreme ultraviolet and soft X-ray imaging) it has proven its usefulness.

As a recent result of such studies, it has been found that CMEs associated with dekametric/hectometric type II bursts are faster and also wider than the average (Gopalswamy et al. 2000). This is a particularly good indicator of geo-effectiveness.

5.3 Studying and Tracking Interplanetary Disturbances

The final approach of using radio data for space weather purposes is more direct: we can directly observe the disturbances which may become geo-effective as they propagate away from the Sun, through the IP medium, towards the Earth. Here, low-frequency observations that require radio receivers aboard spacecraft are employed. It should be noted that this is presently the *only* way to track such disturbances between the high corona, where they may still be observable with a coronagraph, and 1 AU. IP disturbances may be measured in-situ, but that is usually possible only near the Earth, and even then only at a few points at best.

IP type III bursts are the most common feature in the long-wavelength regime. While the electrons producing them can reach the Earth, they are not energetic enough to cause significant space weather effects. However, they offer very important diagnostics of the propagation of particles through the IP medium. As an example, Reiner et al. (1998a) used the radiospectrographs aboard the widely separated Ulysses and Wind spacecraft to reconstruct the 3-D trajectory of an IP type III burst. With these observations, it was also possible to measure the IP plasma density along the path of the radio source.

In terms of relevance to space weather, the study of type II bursts offers us the most interesting and extensive information. Fast CMEs (with velocities of up to 2000 $\mathrm{km\,s^{-1}}$) are highly associated with both SEP events and IP shocks (see Sect. 1), and consequently, with IP type II bursts (e.g. Gopalswamy et al. 2000). Dekametric/hectometric/kilometric observations with space-based radiospectrographs allow the identification of shock-driving CMEs, and the tracking of the IP type II emission lanes from the high corona up to 1 AU. Combined with a heliospheric density model (e.g. Mann et al. 1999), this yields the distance between shock and Sun and the shock's velocity (Reiner et al. 1998b). These parameters are a vital input to the models which are used to predict the arrival time of IP shocks and their associated CMEs (see, e.g., Fry et al. 2003).

Another interesting discovery was that when a fast CME overtakes a slower one, an interaction takes place which shows up as an intense radio continuum superposed on the type II lane (Gopalswamy et al. 2001). This enhancement is interpreted as a consequence of shock strengthening. The CME interaction has important implications for space weather: since the trajectories of the interacting CMEs can change significantly, this process might be responsible for many false alarms when predicting CME or shock arrivals at the magnetosphere.

A totally different method of tracking ICMEs is the interplanetary scintillation (IPS) technique (Hewish et al. 1964). It exploits the scattering of radiation from pointlike radio sources (extragalactic objects, i.e. quasars) by small-scale density inhomogeneities in the IP medium. Thus, it is possible to track the compression region (which is associated with enhanced turbulence) between the IP shock which propagates in front of the ICME and the ICME body. The IPS technique provides the speed and the level of density fluctuations of the disturbance, while the observation of a large number of radio sources provides a good spatial resolution. For a recent application of the technique, see Manoharan et al. (2000).

6 Conclusion

Solar non-thermal radio radiation is a valuable tool for studying solar activity, in particular with respect to the solar eruptive phenomena (flares and CMEs) that are the main drivers of space weather. Observations at shorter wavelengths (microwaves to meter waves) provide information on the primary energy release and particle acceleration in flares, as well as on the initial development of CMEs and smaller-scale ejecta (i.e. plasmoids) and associated phenomena, such as shock waves. Type III bursts (electron beams) are sensitive signatures of energy release and particle acceleration in the corona. Type II bursts track shock waves that are generated by flares (pressure pulse) and/or CMEs (piston mechanism). In summary, radio obseravtions at shorter wavelengths are employed to study the basic physics of the main solar driver of space weather, as well as the phenomena associated with these eruptive events (i.e. coronal waves and shocks, ejecta, particle beams).

At longer wavelengths (dekameter to kilometer waves), the whole height range from the upper corona, through the IP medium, up to and beyond the Earth can be observed. It is in this range where the main causes of geomagnetic disturbances develop and propgagate towards the Earth: fast CMEs drive IP shock waves, which are believed to be primarily responsible for the SEP events that can lead to severe geo-effective consequences. On the other hand, the CMEs themselves, upon reaching the Earth, can interact with the terrestrial magnetosphere, leading to a geomagnetic storm. Using space-borne radio receivers operating in the dekameter to kilometer wavebands, these disturbances can be tracked from the high corona up to the Earth.

As our technical civilization becomes increasingly vulnerable to space weather hazards, the reliability of forecasts has to be increased significantly. In this process, radio data will be a major contribution. A new generation of solar radio instruments is currently under study and/or development. Two projects for ground-based observatories – the Frequency-Agile Solar Radiotelescope (FASR) and the Low Frequency Array (LOFAR) – combine spectral resolution with imaging capability and high time cadence. With these assets,

substantial advances in our understanding of solar eruptive events and their consequences for the Earth are to be expected.

Acknowledgements

The work of A. Warmuth was supported by DLR under grant No. 50 QL 0001. We thank H.-T. Classen for the preparation of figures. The data and software for the hard X-ray and particle observations were provided by the RHESSI and Wind/3DP Investigation teams (R. P. Lin, PI) at the University of California, Berkeley. The radio spectrum from the Ondřejov Obseravtory is by courtesy of M. Karlický.

References

1. Aurass, H., Hofmann, A., & Urbarz, H.-W.: Astron. Astrophys. **334**, 289 (1998)
2. Bastian, T. S., Pick, M., Kerdraon, A., Maia, D., Vourlidas, A.: Astrophys. J. **558**, L65 (2001)
3. Bougeret, J.-L., Kaiser, M. L., Kellogg, P. J., et al.: Space Sci. Rev. **71**, 231 (1995)
4. Bougeret, J.-L., Zarka, P., Caroubalos, C., et al.: Geophys. Res. Lett. **25**, 2513 (1998)
5. Burlaga, L. F., Sittler, E., Mariani, F., & Schwenn, R.: J. Geophys. Res. **86**, 6673 (1981)
6. Cane, H. V., Stone, R. G., Fainberg, J., et al.: Geophys. Res. Lett. **8**, 1285 (1981)
7. Cane, H. V., Sheeley, N. R., Jr., & Howard, R. A.: J. Geophys. Res. **92**, 9869 (1987)
8. Chen, J., Cargill, P. J., & Palmadesso, P. J.: J. Geophys. Res. **102**, A7-14701 (1997)
9. Classen, H. T., & Aurass, H.: Astron. Astrophys. **384**, 1098 (2002)
10. Classen, H. T., Mann, G., Klassen, A., & Aurass, H.: Astron. Astrophys. **409**, 309 (2003)
11. Cliver, E. W., Webb, D. F., & Howard, R. A.: Solar Phys. **187**, 89 (1999)
12. Fry, C. D., Dryer, M., Smith, Z., Sun, W., Deehr, C. S., & Akasofu, S.-I.: J. Geophys. Res. **108**, SSH 5-1/2002JA009474 (2003)
13. Gary, D. E., & Hurford, G. J.: Astrophys. J. **420**, 903 (1994)
14. Gopalswamy, N., & Kundu, M. R.: Astrophys. J. **365**, L31 (1990)
15. Gopalswamy, N., & Hanaoka, Y.: Astrophys. J. **498**, L179 (1998)
16. Gopalswamy, N., Kaiser, M. L., Lepping, R. P., et al.: J. Geophys. Res. **10**, 307 (1998)
17. Gopalswamy, N., Kaiser, M. L., Thompson, B. J., et al.: Geophys. Res. Lett. **27**, 1427 (2000)
18. Gopalswamy, N., Yashiro, S., Kaiser, M. L,; Howard, R. A., & Bougeret, J.-L.: Astrophys. J. **548**, L91 (2001)
19. Gosling, J. T.: J. Geophys. Res. **98**, 18937 (1993)
20. Hanaoka, Y., Kurokawa, H., Enome, S., et al.: PASJ **46**, 205 (1994)

21. Hewish, A., Scott, P. F., & Wills, D.: Nature **203**, 1214 (1964)
22. Jiricka, K., Karlický, M., Kepka, O., & Tlamicha, A.: Solar Phys. **147**, 203 (1993)
23. Kahler, S. W., & Reames, D. V.: Astrophys. J. **584**, 1063 (2003)
24. Kerdraon, A., & Delouis, J.-M.: The Nançay Radioheliograph. In: *Coronal Physics from Radio and Space Observations*, ed. by Trottet, G. (Springer, Berlin Heidelberg New York 1997), Vol. 483 of LNP, p 192
25. Klassen, A., Bothmer, V., Mann, G., Reiner, M. J., Krucker, S., Vourlidas, A., & Kunow, H.: Astron. Astrophys. **385**, 1078 (2002)
26. Koutchmy, S.: Adv. Space Res. **14 (4)**, 29 (1994)
27. Kundu, M. R., Schmahl, E. J., Gopalswamy, N., White, S. M.: Adv. Space Res. **9 (4)**, 41 (1989)
28. Lin, R. P., Anderson, K. A., Ashford, S., et al.: Space Sci. Rev. **71**, 125 (1995)
29. Lin, R. P., Dennis, B. R., Hurford, G. J., et al.: Solar Phys. **210**, 3 (2002)
30. Maia, D., Pick, M., Vourlidas, A., Howard, R.: Astrophys. J. **528**, L49 (2000)
31. Mann, G., Aurass, H., Voigt, W., & Paschke, J.: in Proc. 1st *SOHO* Workshop, ESA SP-348, 129 (1992)
32. Mann, G.: Theory and Observations of Coronal Shock Waves. In: *Coronal Magnetic Energy Releases*, ed. by Benz, A., & Krüger, A. (Springer, Berlin Heidelberg New York 1995), Vol. 444 of LNP, pp 183–200
33. Mann, G., Jansen, F., MacDowall, R. J., Kaiser, M. L. & Stone, R. G.: Astron. Astrophys. **348**, 614 (1999)
34. Mann, G., Classen, H. T., Keppler, E., & Roelof, E. C.: Astron. Astrophys. **391**, 749 (2002)
35. Mann, G., Klassen, A., Aurass, H., & Classen, H. T.: Astron. Astrophys. **400**, 329 (2003)
36. Manoharan, P. K., Kojima, M., Gopalswamy, N., Kondo, T., & Smith, Z.: Astrophys. J. **530**, 1061 (2000)
37. Manoharan, P. K., Tokumaru, M., Pick, M., et al.: Astrophys. J. **559**, 1180 (2001)
38. McLean, D. J., & Labrum, N. R.: *Solar Radiophysics*, (Cambridge Univ. Press, Cambridge 1985)
39. Melrose, D. B.: Plasma emission mechanisms. In: *Solar Radiophysics*, ed. by McLean, D. J., & Labrum, N. R. (Cambridge Univ. Press, Cambridge 1985), pp 177–210
40. Nakajima, H., Nishio, M., Enome, S., et al.: Proc. IEEE **82**, 705 (1994)
41. Newkirk, G. A.: Astrophys. J. **133**, 983 (1961)
42. Radick, R. R.: Proc. SPIE **4498**, 84 (2001)
43. Reames, D. V.: Space Sci. Rev. **90**, 413 (1999)
44. Reiner, M. J., Fainberg, J., Kaiser, M. L., & Stone, R. G.: J. Geophys. Res. **103**, 1923 (1998)
45. Reiner, M. J., Kaiser, M. L., Fainberg, G. J., & Stone, R. G.: J. Geophys. Res. **103**, 29651 (1998)
46. Shanmugaraju, A., Moon, Y.-J., Dryer, M., & Umapathy, S.: Solar Phys. **215**, 161 (2003)
47. Smerd, S. F., Sheridan, K. V., & Stewart, R. T.: Astrophys. J. **16**, 23L (1975)
48. Stewart, R.T.: Solar Phys. **94**, 379 (1984)
49. Stewart, R.T.: Moving Type IV Bursts. In: *Solar Radiophysics*, ed. by McLean, D. J., & Labrum, N. R. (Cambridge Univ. Press, Cambridge 1985), pp 361–383

50. Vršnak, B., & Lulić, S.: Solar Phys. **196**, 157 (2000)
51. Vršnak, B., & Lulić, S.: Solar Phys. **196**, 181 (2000)
52. Vršnak, B.: J. Geophys. Res. **106**, 25249 (2001)
53. Vršnak, B., Aurass, H., Magdalenić, J., & Goplswamy, N.: Astron. Astrophys. **377**, 321 (2002)
54. Vršnak, B., Magdalenić, J., Aurass, H., & Mann, G.: Astron. Astrophys. **396**, 673 (2002)
55. Warmuth, A., Vršnak, B., Aurass, H., & Hanslmeier, A.: Astrophys. J. **560**, L105 (2001)
56. Webb, D. F.: Rev. Geophys. Suppl. **33**, 577 (1995)